International Journal of Neural Systems, Vol. 23, No. 6 (2013) 1350025 (17 pages)

DOI: 10.1142/S0129065713500251

World Scientific
www.worldscientific.com

A GRAY-BOX NEURAL NETWORK-BASED MODEL IDENTIFICATION AND FAULT ESTIMATION SCHEME FOR NONLINEAR DYNAMIC SYSTEMS

ZHAOHUI CEN* and JIAOLONG WEI†,‡
Department of Electronic and Information Engineering
Huazhong University of Science and Technology
Wuhan, China
**cenzhaohui@gmail.com*
†*jlwei@mail.hust.edu.cn*

RUI JIANG
Smart Transport Research Center
Civil Engineering and Built Environment School
Science and Engineering Faculty
Queensland University of Technology
Queensland, Australia
jerrken@gmail.com

Accepted 18 June 2013
Published Online 23 July 2013

A novel gray-box neural network model (GBNNM), including multi-layer perception (MLP) neural network (NN) and integrators, is proposed for a model identification and fault estimation (MIFE) scheme. With the GBNNM, both the nonlinearity and dynamics of a class of nonlinear dynamic systems can be approximated. Unlike previous NN-based model identification methods, the GBNNM directly inherits system dynamics and separately models system nonlinearities. This model corresponds well with the object system and is easy to build. The GBNNM is embedded online as a normal model reference to obtain the quantitative residual between the object system output and the GBNNM output. This residual can accurately indicate the fault offset value, so it is suitable for differing fault severities. To further estimate the fault parameters (FPs), an improved extended state observer (ESO) using the same NNs (IESONN) from the GBNNM is proposed to avoid requiring the knowledge of ESO nonlinearity. Then, the proposed MIFE scheme is applied for reaction wheels (RW) in a satellite attitude control system (SACS). The scheme using the GBNNM is compared with other NNs in the same fault scenario, and several partial loss of effect (LOE) faults with different severities are considered to validate the effectiveness of the FP estimation and its superiority.

Keywords: Model identification and fault estimation; nonlinear dynamic systems; gray-box neural-network model; extended state observer; reaction wheel.

1. Introduction

Improving the security and reliability of man-made dynamic systems has become more and more critical over the past two decades. The requirements for such systems are now extending beyond the safety-critical systems of nuclear reactors, engines, high-rise buildings, chemical plants and aircrafts to new systems, such as autonomous vehicles[1–6] and the human body system.[7,8] For all these systems, fault diagnosis (FD) is an essential reliability approach that can

‡Corresponding author.

help avoid system shutdown, breakdown and even catastrophes involving human fatalities and material damage. Over the past three decades, many approaches to FD have been proposed, including a model-based approach,[9] a computing-intelligence-based approach[10,11] and a hybrid approach.[12]

Neural networks (NN)-based FD method is a representative of the computing-intelligence-based approach. Compared with the model-based FD method, NN-based FD does not require detailed information of the object system, such as structure and parameters. Not only an effective optimization method,[13–22] the NN is also an ideal mathematical tool for FD applications owing to its universal nonlinear function approximation property and its ability to learn and reproduce system behavior from quantitative system datasets (i.e. historical system input–output data).[23,24] Accordingly, NN has been extensively applied to FD, which include the NN-based pattern recognition approach,[25] NN-based residual generation decision-making scheme,[26] and NN-based multiple-model residual generation and classification.[27] The last two approaches, which use residuals for FD, dominate the field implementation. The residual is derived from a NN-based identification model, and is then used to detect fault or even to estimate fault if accurate sufficiently. The more accurate the identification model is, the higher quality of the residual is; therefore, NN-based identification is fundamental for NN-based FD.

The NN is an ideal tool of model identification (MI) for nonlinear systems. Numerous studies have been conducted on the FD for nonlinear dynamic systems using NN-based MI. However, only few studies have utilized the identified NN model to accomplish fault estimation (FE). Three categories of NN-based nonlinear dynamic system identification schemes have been developed. The first category is called static NN such as multi-layer perception (MLP) NN.[28] The second category is called dynamic NN because these NNs have integrators or delay components in their structure.[29–40] Generally, a single dynamic NN is used to model the object system; thereafter, it is trained offline. The third category is online NN observers. Kim[41] studied on an NN observer using dynamic recurrent NNs, which can only estimate the system states. Talebi[42] presented a hybrid intelligent fault detection and isolation scheme for a general nonlinear system using an NN-based observer. However, these works have not addressed the estimation of fault severity. In Refs. 43 and 44, a hybrid FD approach was presented to estimate the fault parameter (FP) vector and fault severities, using a bank of parameterized fault models and a corresponding bank of adaptive neural parameter estimators. However, *priori* knowledge of faults and system nonlinearity is required to predefine the parameterized fault models. In addition, online generalization is an inherent problem for the neural parameter estimators.

Model accuracy is one of the most crucial factors for MI, particularly for model-based FD. If a residual is sufficiently accurate to differ the fault severities, this FD scheme is aptly called FE — a challenging problem encountered in the FD research field.

To identify a nonlinear dynamic system is to approximate nonlinearity and dynamics simultaneously. The nonlinearity reflects the static behavior, whereas the dynamics reflects the dynamic behavior. For simple object systems, white-box modeling, such as a model observer, is typically used to perform FD, because the structure and physical principles are normally known. However, most practical systems are actually complicated, with unknown or partially unknown structures and physical principles. In this case, white-box modeling is not applicable. Compared with white-box modeling, black-box modeling methods, such as the NN-based identification and Wiener–Hammerstein models,[45,46] do not require the knowledge of structure and physical principles. However, it is difficult to train models with desired accuracy for nonlinear dynamic systems. Currently, the training of NN is based on samples, and samples are individual behaviors. The static behaviors are included in the samples, so NN can learn from the training. However, the system dynamics, the relationship between individual samples, are not included. Consequently, the system dynamics cannot be trained. This is why the dynamic structure is predefined in dynamical NN rather than trained. In some cases, the knowledge of the system dynamics is known, which can be utilized naturally to improve model accuracy so as to implement FE.

With this motivation, a novel gray-box neural network model (GBNNM) method, which mixes both white-box and black-box approaches, is proposed. Because the GBNNM can produce high-quality residual, it is suitable to estimate the fault severity. To

estimate the partial loss of effect (LOE) FPs, an improved extended state observer (ESO) using the same NNs from the GBNNM is developed, which does not require the knowledge of observer nonlinearity and provides a more visual FE result.

The contributions of this paper are to present a sufficiently accurate NN model and a novel ESO to fulfill FE. Unlike many previous NN-based identification methods,[29–34,37,38,42,47] this method does not adopt a single NN to model an object system in a black-box manner. Instead, it uses multiple static NNs to approximate corresponding nonlinearities separately, to decrease the complexity of identification. Compared with other multi-model FD approaches,[27,48] redundant fault models are not required to generate multiple residuals for fault severity estimation. Compared with the FE approach,[43,44] the GBNNM can be trained offline, and thus, it can avoid the problems with online generalization. In contrast to our previous studies in computing-intelligence-based FD,[49,50] the GBNNM is used not only to detect faults but also to estimate fault severity and even FPs. In addition, in contrast to our previous studies on model observers,[51] the GBNNM is used as a normal model reference instead of an analytical model, and an improved ESO derived from the GBNNM is proposed.

The remainder of this paper is organized as follows. The problem and some concepts are first introduced in Sec. 2. In Sec. 3, MI using the proposed GBNNM is presented, and its approximate ability is analyzed theoretically. In Sec. 4, FE based on a GBNNM model estimator and improved ESO with NN is presented. In Sec. 5, an example of an MIFE and the corresponding experiments result are presented using a high-resolution single-input-single-output (SISO) reaction wheel (RW) model. The conclusions and highlights are provided in Sec. 6.

2. Problem Formulation and Concept

2.1. *FE problem*

To implement condition-based maintenance, such as fault accommodation, requires an accurate FD: that is, to compare the system with another normal system under identical operational conditions. This comparison is called the peer-to-peer concept in the FD field. For example, the fault can be detected, and the offset value between the fault mode and normal mode can reflect the severity of the fault (also called FE) based on the desired residual at the bottom left of Fig. 1. However, constructing the reference system for FE is not cost effective. An alternative solution is to use simulation model. However, the residual in the lower right of Fig. 1 illustrates that it is easy to detect faults but not to estimate them because the residual is not sufficiently accurate for FE. Therefore, the key is to precisely identify or construct a simulation model.

2.2. *Identification problem of the nonlinear dynamic system*

An example of nonlinear dynamic system is shown in Fig. 2. It includes both nonlinearities and dynamics. The nonlinearities are the functions in Fig. 2, i.e. $f_1 \cdots f_4$, whereas the dynamics are the integrators and its connection to the nonlinear functions. The nonlinearities and dynamics are coupled in the model structure. In general, there are two identification approaches, namely the white-box and black-box approach.

On one hand, the white-box approach is used when full knowledge of both the nonlinearity and dynamics of the system are available. The identification process involves obtaining the unknown parameters or variables in the white-box model. However, its drawback is the requirement of full *priori* knowledge of the object system, making it unsuitable for complicated real system.

On the other hand, the black-box approach is generally used when no knowledge of the object system is available. The black-box approach defines a general and known model structure with parameters for identification. The advantage of the black-box approach is no requirement of full knowledge. However, when applied in identification of nonlinear dynamic systems, obtaining a model with sufficient accuracy to approximate nonlinearity and dynamics simultaneously is difficult.

At present, there are the four types of NN that can be applied to FD. These NNs include Series-Parallel NARX NN (SPNN), Parallel NARX NN (PNN), Recurrent NN (RNN) and Static MLP NN (SNN), all of which are embedded to implement residual-based FD. A representative example of offline identification by an SPNN is provided in Fig. 3 to illustrate the identification principle and drawbacks of these NNs.

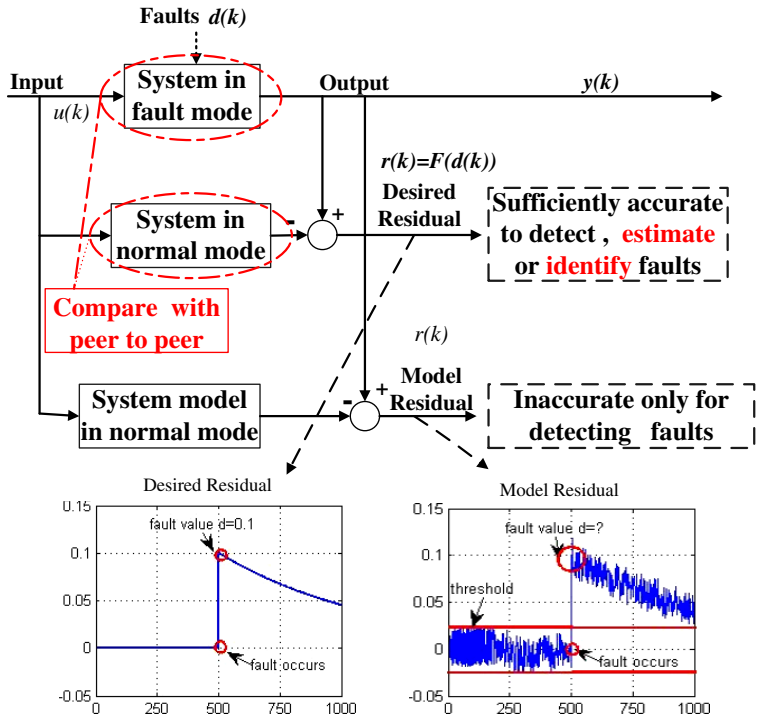

Fig. 1. FD based on comparing with peer to peer.

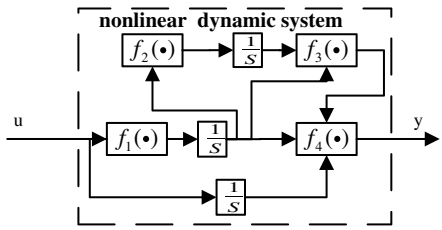

Fig. 2. An example of nonlinear dynamic system.

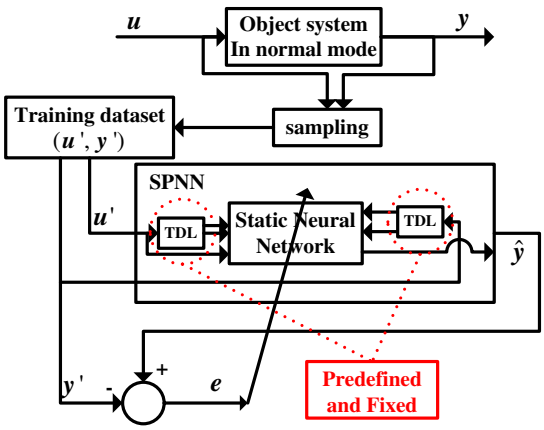

Fig. 3. NN offline identification by an SPNN.

As shown in Fig. 3, the objective of the NN training algorithm is to minimize the error between the sample output y' and the corresponding NN model output $\hat{y}$ estimation. The training algorithm adopts some parameter-searching strategy, such as the Levenberg–Marquardt (LM) back-propagation training function and the gradient descent (GD) with momentum weight/bias learning function,[52] to adjust the parameters of all neurons in the static NN of Fig. 3. These parameters include two classes, namely, weight and bias. The dynamic elements in the tapped delay line (TDL) cannot be changed during the training process, as TDLs are fixed for a specified NN. The fixed structure can help avoid the requirement for knowledge about the object system. However, a fixed structure is not sufficiently flexible to match the dynamics of the object system, even if it matches the nonlinearity of the object system well. In some cases, the fixed structure has a negative effect on matching the nonlinearity of the object system. In fact, the training process aims to learn the static behavior from the training sample rather than to learn both the static and dynamic behavior. The unmatched dynamics would

decrease the performance of estimating nonlinearity when applying online, because the nonlinearity and dynamics are coupled in nonlinear dynamic systems.

Moreover, for an industrial system, some information is generally known *a priori*. This information might be the probability density function, general statistics of the process data, impulse response or attractor geometry or the underlying physics.[52,53] Because black-box modeling requires no knowledge of the object system, *a priori* information is not used and thereby wasted. With this information used in the context of gray-box modeling, it is expected to be able to approximate nonlinearity and dynamics simultaneously so that the model has sufficient accuracy for FE.

3. Gray-Box NN Identification of a Nonlinear Dynamic System

3.1. *System description and the identified model structure*

Owing to the popularity of first-order systems, the identification of nonlinear dynamic systems is considered with the following general form:

$$\begin{cases} \dot{x} = F(x,u) \\ y = h(\dot{x},x), \end{cases} \tag{1}$$

where $x \in \Re^n$ is the state vector, $u \in \Re^m$ is the system input and $y \in \Re^p$ is the output vector of the system. $F(x,u)$ and $h(\dot{x},x)$ represent unknown constitutive nonlinearities. The coupling relationship and dynamics are easy to obtain for a nonlinear system in the form of (1) because only one integrator is included in the dynamics.

The gray-box approach presented would preserve the model structure inherent in (1) without requiring *a priori* representations of the nonlinearities $F(x,u)$ and $h(\dot{x},x)$. Instead, these terms would be represented by a separate MLP feed-forward NN $g_1(\hat{x},u,w_1)$ and $g_2(\hat{x},\dot{\hat{x}},w_2)$:

$$\begin{aligned} \dot{\hat{x}} &= g_1(\hat{x},u,w_1), \\ \hat{y} &= g_2(\hat{x},\dot{\hat{x}},w_2). \end{aligned} \tag{2}$$

By modeling the nonlinearities $F(x,u)$ and $h(\dot{x},x)$, the model structure of (2) is preserved. The MLP feed-forward NN is utilized to approximate nonlinearity, so $g_1(x,u,w_1)$ and $g_2(x,\dot{x},w_2)$ can be denoted as

$$\begin{aligned} g_1(x,u,w_1) &= W_{11}\sigma(\theta_1 + W_{12}p_1) \\ g_2(x,\dot{x},w_2) &= W_{21}\sigma(\theta_2 + W_{22}p_2), \end{aligned} \tag{3}$$

where $\sigma(\cdot)$ is the activation function of the hidden-layer neurons that is typically set to be a sigmoid function.

$$\begin{cases} \sigma(\theta_1 + W_{12}p_1) = \dfrac{2}{1+\mathrm{e}^{-2(\theta_1+W_{12}p_1)}} - 1 \\ \sigma(\theta_2 + W_{22}p_2) = \dfrac{2}{1+\mathrm{e}^{-2(\theta_2+W_{22}p_2)}} - 1, \end{cases} \tag{4}$$

where $p_1 = [x,u]^T$ and $p_2 = [x,\dot{x}]^T$ are the inputs of two NNs. The weight parameters $w_1 = [W_{11}\ W_{12}\ \theta_1]$ and $w_2 = [W_{21}\ W_{22}\ \theta_2]$ are the parameters of the two NNs.

This gray-box approach preserves the direct associations between the NN's architecture and its weights to the underlying systems' dynamics. For a general nonlinear dynamic system in the form of (1), MLP feed-forward NN $g_1(x,u,w_1)$ and $g_2(x,\dot{x},w_2)$ are just used to approximate the nonlinearities $F(x,u)$ and $h(\dot{x},x)$. The relationship between $x(t)$ and $\hat{x}(t)$, which is the solutions of (1) and (2), is uncertain. Furthermore, the relationship between $y(t)$ and $\hat{y}(t)$, which are outputs of (1) and (2), respectively, is uncertain. To analyze the relationship between (1) and (2), some preliminaries and proofs will be provided in Sec. 3.2.

3.2. *Analyses of approximation ability*

Lemma 1. *Let $S \subset \Re^n$ and $U \subset \Re^m$ be open sets, $X \subset S$ and $D_U \subset U$ be compact sets, and mapping $F : S \times U \to R^n$ be a C^1-class function. If a continuous nonlinear system is in the form*

$$\begin{cases} \dot{x}(t) = F(x(t),u(t)) \\ y(t) = h(\dot{x}(t),x(t)) \end{cases} \quad x \in S,\ \ u \in U,\ \ t \in [0,T],\ \ (0 < T < \infty) \tag{5}$$

with an initial state $x(0) \in X$, then for an arbitrary $\varepsilon > 0$, there exists an integer N and a GBNNM of form (6) *with an approximate initial condition*

$x(t_0) = \hat{x}(t_0) \in S$.

$$\begin{cases} \dot{\hat{x}}(t) = g_1(\hat{x}(t), u(t)) \\ \qquad = A_1\sigma(B_{11}x + B_{12}u + \theta_1) \\ \hat{y}(t) = g_2(\dot{\hat{x}}(t), \hat{x}(t)) \\ \qquad = A_2\sigma(B_{21}x + B_{22}u + \theta_2) \end{cases} \tag{6}$$

such that for any bounded input $u(t) \in D_U, t \in [0, T]$.

$$\max_{t\in[0,T]} \|y - \hat{y}\| < \varepsilon. \tag{7}$$

According to Lemma 2 in 49, there exists an integer N_2 and an MLP NN of formula (3) with an N_2-dimensional threshold θ_2 and matrices $A_2 \in \Re^{n\times N_2}$, $B_{21} \in \Re^{N_2\times n}$ and $B_{22} \in \Re^{N_2\times m}$. For an arbitrary $\varepsilon_2 > 0$:

$$\|h(\hat{x}, \hat{x}) - A_2\sigma(B_{21}\hat{x} + B_{22}u + \theta_2)\| \le \varepsilon_2 = \frac{\varepsilon}{2}. \tag{8}$$

According to Corollary 1 in 49, there exists an integer N_1 and an MLP NN of formula (3) with an N_1-dimensional threshold θ_1 and matrices $A_1 \in \Re^{n\times N_1}$, $B_{11} \in \Re^{N_1\times n}$ and $B_{12} \in \Re^{N_1\times m}$. $x(t)$ and $\hat{x}(t)$ are the solutions of the differential equations in (5) and (6), respectively, with the initial condition $x(t_0) = \hat{x}(t_0) \in S$.

***Comment*:** The above lemma reflects a constructive way to create a GBNNM that has universal approximation capability for a nonlinear dynamic system. From the theoretical analysis of the GBNNM, we can see that different nonlinearities in the system can be separately approximated by MLP NNs. Importantly, the complexity of identification is decomposed, so the GBNNM can be constructed in steps.

3.3. *Training algorithm with a self-defined exciting strategy*

To train a NN model with better generality performance, a self-defined exciting strategy is introduced to obtain sample data for training.[50] Based on using band-pass Gaussian white noise as the exciting input and the corresponding system output, a NN model can be obtained for approximation. Therefore, the offline identification can be divided into two steps, as described in Fig. 4.

***Comment*:** To improve the data condition for better approximation and training, a re-sampling for dataset $\{u_t, x, \dot{x}, y_t\}$ is adopted to ensure that the computing time for training is not very long. According to our experience, a final dataset with 1000–10,000 points is suitable for NN training. With the network structures of NN1 and NN2 defined, the LM back-propagation training function and GD with a momentum weight/bias learning function, which are detailed in the Matlab NN Toolbox, are employed to obtain the desired convergence performance.[54]

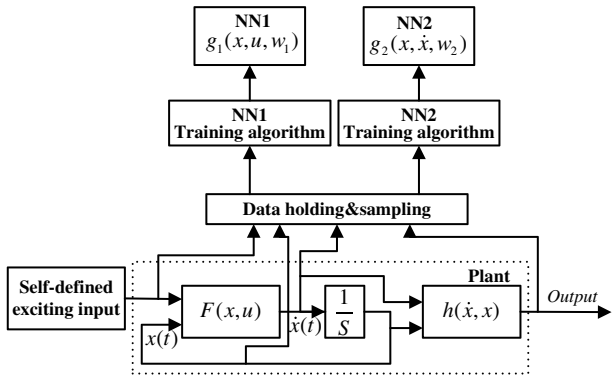

Fig. 4. Offline identification scheme with a self-defined exciting strategy.

4. FE Based on the GBNNM and IESONN

After all of the NN models have been trained offline, a complex structure of FE, including a GBNNM model estimator and an improved ESO based on NNs from the GBNNM, is proposed, as illustrated in Fig. 5. The FE scheme has two outputs, including the GBNNM residual and FP estimation. The GBNNM residual can be used for fault detection or even fault severity identification (called a rough FE), and the improved ESO based on NN (IESONN) estimates FP for further diagnosis (called an accurate FE). The two NNs in the improved ESO utilize the two sub-NNs of the GBNNM to allow the improved ESO to estimate the FP without requiring the knowledge of the nonlinearity in the object system.

4.1. *Fault severity identification based on the GBNNM model residual*

To formulate the fault severity identification result, a residual is defined as:

$$r(t) = y(t) - \hat{y}(t). \tag{9}$$

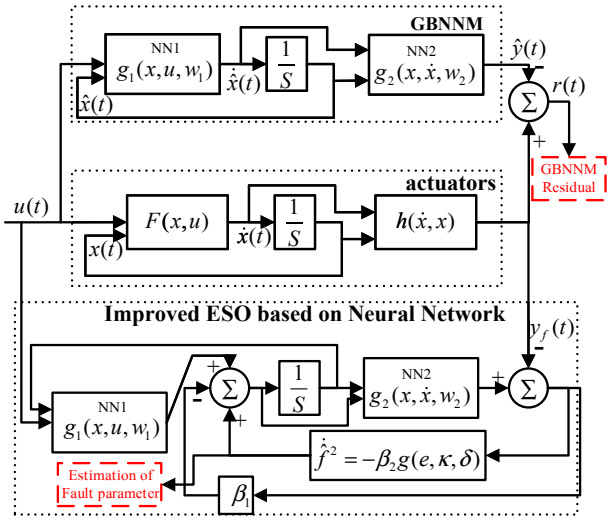

Fig. 5. FE based on GBNNM and IESONN.

We can denote FE (only fault severity identification) based on the GBNNM as:

$$r = \begin{cases} y_n(u) - \hat{y}(u) = 0 & (no\ fault) \\ y_{fo}(u) - \hat{y}(u) = m_1(d_1) & (output\ fault) \\ y_{fo}(u) = y_n(u) + d_1 & \\ y_{fi}(u) - \hat{y}(u) = m_2(d_2) & (input\ fault) \\ y_{fo}(u) = y_n(u + d_2), & \end{cases}$$

where $y_n(u)$ denotes the input–output function of the object system in normal mode. $\hat{y}(u)$ denotes the input–output function of the GBNNM model, $y_{fo}(u)$ denotes the input–output function of the object system in fault mode with an output offset value d_1, and $y_{fo}(u)$ denotes the input–output function of the object system in fault mode with an input offset value d_2.

The residual r equals to zero when no fault occurs. When a fault occurs, all system faults can be classified into two types of equivalent faults, a fault with an output offset or a fault with an input offset, because once a fault exists, it will certainly affect the output or input of a system.

For both fault modes with an output offset and fault modes with an input offset, the residual r is the function of fault value d, which is denoted as $m_1(d)$ or $m_2(d)$. If the fault value d changes, the residual r will change. For a fault mode with an output offset, $r = m_1(d_1) = d_1$. Therefore, we can use this principle to differentiate fault severity. The FE effects will be demonstrated with simulations, as presented in Sec. 5.

***Discussion*:** The residual is the basis of FD. If the distinction between the occurrences of single- and multiple-component failures is required, some preconditions should be satisfied, the effects on the system output in normal mode, single-component failure mode and multiple-component failure mode must be different. Thus, the symptom must be different in different modes. Once the precondition above is satisfied, the GBNNM residual can take on different values in the time domain. Therefore, it is possible to distinguish between the occurrences of single- and multiple-component failures. Whether these types of failure can be distinguished clearly depends on the ability to identify the difference in the failure symptom. If this difference is not obvious in the time domain, a time-frequency signal-processing tool, such as wavelet analysis, is often used to post-process the GBNNM residual to make this difference sufficiently discernible.

4.2. *FP estimation for partial LOE fault*

In the case that the object system is a type of actuator and the fault is a type of partial LOE fault, the FP estimation is generally essential for ensuring the reliability and integrity of the control system. If the object system is a type of actuator but the fault is a type of full LOE fault, the FE is not needed, and a redundant system is generally employed. Therefore, FP estimation for partial LOE faults was studied in our research.

Without loss of generality, we consider a type of partial LOE fault for nonlinear dynamic system (1) in the form

$$\begin{cases} \dot{x} = F_1(x, u_{\text{in}}) + f^2 \\ u_{\text{out}} = h_1(\dot{x}, x) \end{cases}, \tag{10}$$

where f^2 is the fault value, x is the state of the system, u_{in} is the system input, and u_{out} is the system output.

To estimate the fault value f^2, an improved ESO based on NN is proposed in the following format:

$$\begin{cases} e = NN_1(\dot{\hat{x}}, \hat{x}) - u_{\text{out}} \\ \dot{\hat{x}} = NN_2(\hat{x}, u_{\text{in}}) + \hat{f}^2 - \beta_1 e \\ \dot{\hat{f}}^2 = -\beta_2 g(e, \kappa, \delta), \end{cases} \tag{11}$$

where $\beta_1 > 0, \beta_2 > 0$ and $0 < \kappa < 1$. $g(e, \kappa, \delta)$ is a nonlinear continuous function in the form of (12):

$$g(e, \kappa, \delta) = \begin{cases} |e|^{\kappa}\text{sgn}(e), & |e| > \delta \\ e/\delta^{1-\kappa}, & |e| < \delta \end{cases}. \tag{12}$$

To analyze the convergence of an improved ESO based on NN, Lemma 2 and Corollary 2 on the convergence of an ESO are presented.

Lemma 2. *Supposing $\dot{f}^2$ is bounded, if β_1, β_2, κ and δ are set and satisfy*[55]

$$\beta_1^2 > 4\beta_2\delta^{\kappa-1}, \tag{13}$$

then the observer (14) *can estimate the states x and the fault variable f^2 asymptotically.*

$$\begin{cases} e = h_1(\dot{\hat{x}}, \hat{x}) - u_{\text{out}} \\ \dot{\hat{x}} = F_1(\hat{x}, u_{\text{in}}) + \hat{f}^2 - \beta_1 e \\ \dot{\hat{f}}^2 = -\beta_2 g(e, \kappa, \delta) \end{cases}, \tag{14}$$

where $\beta_1 > 0, \beta_2 > 0$ and $0 < \kappa < 1$. $g(e, \kappa, \delta)$ is a nonlinear continuous function in the form of (12).

As seen from (14), the unimproved ESO is a model-based estimator method. Its model structure and parameters are given by the nonlinear functions $F_1(x, u_{\text{in}})$ and $h_1(\dot{x}, x)$. Therefore, the availability of the ESO (14) must be based on the availability of the nonlinear function $F_1(x, u_{\text{in}})$ and $h_1(\dot{x}, x)$. As is discussed in Sec. 2, generally, nonlinear relationships are not available for industrial applications. Therefore, the gray-box identification is introduced to obtain an approximation of nonlinear functions.

To estimate the process FP-partial LOE fault value f^2, the NNs in the GBNNM can be used again in the improved ESO to approximate the nonlinear functions $F_1(x, u_{\text{in}})$ and $h_1(\dot{x}, x)$. Therefore, Corollary 2 is given to analyze the convergence of the improved observer of (11).

Corollary 2. *Supposing $\dot{f}^2$ is bounded, if NN1 and NN2 are the nonlinear approximations of $F_1(x, u_{\text{in}})$ and $h_1(\dot{x}, x)$, β_1, β_2, κ and δ are set and satisfy* (13), *then the observer* (11) *can also estimate the states x and the fault variable f^2 asymptotically.*

Proof. According to ***Lemma* 2**, the following approximate equations can be obtained:

$$\begin{cases} F_1(x, y) \approx NN_1(x, y) \\ h_1(\dot{x}, x) \approx NN_2(\dot{x}, x). \end{cases} \tag{15}$$

Therefore, the improved ESO based on NN of (11) has the same convergence as the ESO of (14) with the same error dynamic adjustment. The approximation error is strictly restrained by the high-gain parameter convergence conditions of (13). □

5. Case Study: Application to the RW in SACS

Improvements in the accuracy and reliability of the RW in SACS directly contribute to mission success and performance.[47] Inherent dynamic nonlinearities, however, make the requirement for an accurate and efficient MIFE for the RW of SACS a challenging and nontrivial problem. In this section, an example of a high-fidelity RW in SACS using the proposed MIFE method is presented.

5.1. *High-fidelity RW in SACS*

A type of complete SACS model is considered.[56,57] The structure of the model (see Fig. 6) is composed of a controller, actuator (i.e. RW), satellite attitude dynamics, satellite attitude kinematics, attitude sensors and attitude determination module. The attitude sensor module is composed of a rate-integrating gyro, infrared earth sensors and sun sensors. Related

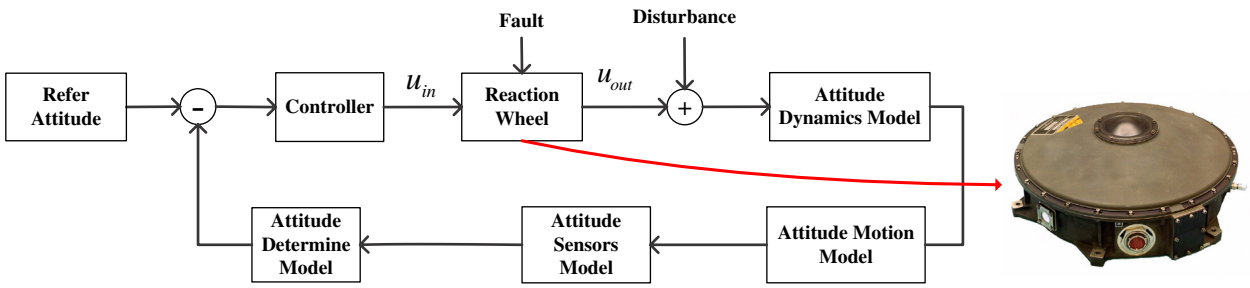

Fig. 6. Block diagram of SACS.

studies on modeling and the real-time simulation effect of SACS are detailed in Ref. 49.

The selection of RWs for attitude control is justified due to their popularity in satellite attitude control. SACS can be considered a MIMO control system whereas the single-axis RW is a SISO system. A high-fidelity nonlinear model of the RW was obtained from Ref. 49 and was integrated into the SACS.

To simulate the object system, two types of disturbances are considered: disturbances outside the RW (see Fig. 6) and disturbances of the friction inside the RW. Both real-time simulations in fault-free and fault modes are performed on the fault diagnosis and tolerant control platform (FDTCP), which is shown in Figs. 7 and 8. The platform was developed by the Space Intelligent Control State Key Lab of China. This platform has been introduced and described in Ref. 58.

Fig. 7. Real-time simulation environment based on FDTCP for attitude and orbit control (AOC).

Fig. 8. Interface matrix device for fault simulation and injection.

5.2. *Faults of the RW*

Without loss of generality, two common RW fault modes are considered. The two fault modes are the augmentation of friction torque and the continuously decreasing angular velocity of the RW. The former is a type of partial LOE Fault, whereas the latter is a type of full LOE fault.

(a) Fault mode 1

The augmentation of friction torque is derived from the disturbance coupling function. Accordingly, the RW output formulation is rewritten as

$$y = \begin{bmatrix} T_c \\ h \end{bmatrix} = f_1(\overline{u_{\text{in}}} + d^1) = \begin{bmatrix} \overline{u_{\text{in}}} + f - \xi(h) \\ \int (\overline{u_{\text{in}}} + f - \xi(h))dt \end{bmatrix}. \tag{16}$$

Changing the value of d^1 depends on the nature of the fault. If the value of d^1 changes into another constant value and stays, it is a sustained fault. If the value of d^1 changes several times and returns to zero, it is an intermittent fault. Without loss of generality, the following intermittent time-varying fault in the disturbance coupling function is injected into the RW on the Pitch axis as a variation.

$$d^1 = \begin{cases} 0 & 0 \le t < 500 \\ 0.1 & 500 \le t < 600 \\ 0.15 & 600 \le t < 700 \\ 0.2 & 700 \le t < 800 \\ 0 & 800 \le t < 1000 \end{cases}. \tag{17}$$

(b) Fault mode 2

The continuous decrease of the angular velocity is derived from the speed limiter function. Accordingly, the RW formulation is rewritten as

$$\begin{cases} u_{\text{out}} = \begin{cases} h(T_c, h); & 0 \le t < T_{d^2} \\ d^2; & T_{d^2} \le t < 1000 \end{cases} \\ h(T_c, h) = \begin{cases} -T_c, & J|\Omega| < h_{\max} \\ 0, & J|\Omega| \ge h_{\max} \end{cases} \end{cases}. \tag{18}$$

Similar to fault mode 1, the following intermittent time-varying fault in the speed limiter function is

injected into the RW on the Pitch axis as a variation.

$$d^2 = \begin{cases} 0 & 0 \le t < T_{d^2} \\ 0.05 & T_{d^2} \le t < 550 \\ 0.08 & 550 \le t < 600 \\ 0.1 & 600 \le t < 650 \\ 0 & 650 \le t < 1000 \end{cases}. \tag{19}$$

5.3. *Experimental results*

To verify the performance of our proposed MIFE scheme, three sets of MIFE simulations are conducted on the FDTCP, and the results are presented in this section. The first set of simulations involves model validation, in which the system state between the object system and GBNNM is compared. The second set of simulations injects specialized faults and verifies the FE performance in different fault modes. The third set of simulations is conducted to compare the performance of our proposed MIFE scheme with other FD methods based on NN identification.

(a) MI Effect Comparison

To quantifiably compare the approximate and generalization ability of the GBNNM with other identification model approaches, two important statistical indexes, R^2 (coefficient of determination) and the root mean square error (RMSE) from the sequence, y and $\hat{y}$, denoted as (20) and (21), are selected. The two indexes for the SNN, RNN, PNN, SPNN and Wiener–Hammerstein models are also computed for comparison.

$$\mathrm{RMSE} = \sqrt{\frac{(y-\hat{y})^{\mathrm{T}} \cdot (y-\hat{y})}{\mathrm{length}(y-\hat{y})}}, \tag{20}$$

$$R^2 = 1 - \frac{\mathrm{RMSE}^2}{\mathrm{VAR}(y)}, \tag{21}$$

where $length(y-\hat{y})$ is the length of sequence $y-\hat{y}$ and $VAR(y)$ is the variance of sequence y.

From the R^2 and RSME of the GBNNM in Table 1, we can see that the GBNNM estimate has good generalizability because the R^2 and RMSE values mostly approximate the desired case and outperform the classical Wiener–Hammerstein nonlinear dynamic model. This result indicates that the GBNNM accurately estimates unknown operating domains even if it is trained to work with limited and known operating points from the sample set.

(b) FE subject to different types of faults

To verify the performance of FE, different fault modes are considered for the second set of simulations. These fault modes include sustained and intermittent faults subject to both LOE faults and partial LOE faults. FE subject to three types of faults is performed in this section.

FE for an LOE sustained fault

The FE results subject to an LOE sustained fault (fault mode 2) with a value of $d^2 = 0.1\,\mathrm{N\cdot m}$ are shown in Fig. 9. Figures 9(a)–9(c) present the responses of the system output, GBNNM model output and residual, respectively. As shown in Fig. 9(a), the jump in the system output response at 500 s demonstrates the effects of fault mode 2. As the action of the closed-loop control law breaks, the response curve tends to be unsteady after 500 s; in other words, the value of the RW output is a nonzero constant, indicating that the system is unstable. Nevertheless, this information alone cannot determine whether a fault has occurred, including its degree of severity. In Fig. 9(b), under the same input and fault effect, the response of the GBNNM model output also jumps at a relative slower speed at 500 s, and the GBNNM model output remains close to the desired model in normal mode. As shown in Fig. 9(c), the response of the output residual approaches zero in the time interval $t \in [0 \quad 500]$. When the fault occurs at 500 s, the value of the residual jumps to a value of 0.1 and then tends to be divergent under the action of system dynamics. Based on a theoretical analysis of the fault nature, the effect of an LOE fault

Table 1. Statistical index for generalization ability.

INDEX	SNN	RNN	PNN	SPNN	GBNNM	Wiener–Hammerstein	Desired
R2	98.84%	−21.25	46.98%	97.46%	99.99%	70.41%	100%
RMSE	3.95e-2	1.73	2.692e-1	5.85e-2	2.7e-3	1.99e-1	0

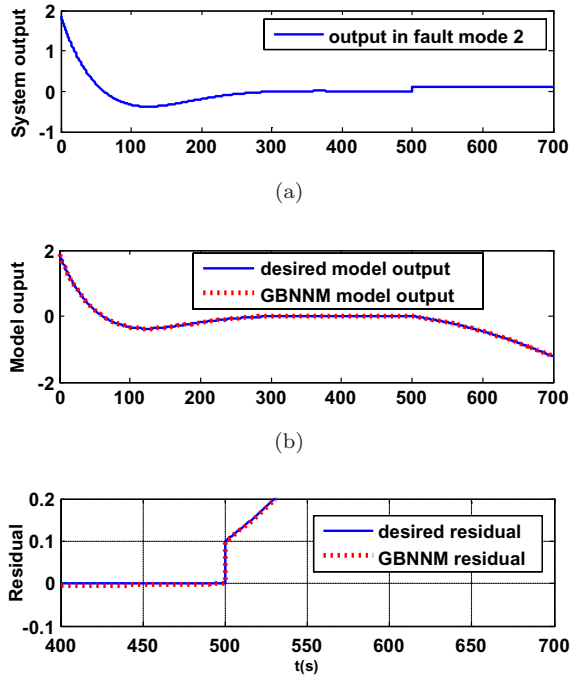

Fig. 9. FE result subjected to fault mode 2. (a) System output, (b) model output comparison between the desired model and GBNNM, and (c) residual comparison between the desired model and GBNNM.

tends to increase under the action of system dynamics after the fault occurs. The residual based on the GBNNM reflects not only the severity of the fault at the occurrence but also the subsequent potential effects after its occurrence.

***Comment*:** Although the SACS is unstable and the output of the RW is discontinuous, the input of the RW, the output of the desired model, and the output of the GBNNM model are still continuous in the fault scenario with the action of closed-loop control. Under the fault scenario, the GBNNM should be the same as the desired model but not the real system. Figure 9(a) illustrates that the object system output in fault mode 2 is discontinuous and unstable. The unstable behavior of the system is because the closed-loop control law is disturbed by the fault effect. However, the discontinuous system output does not change the continuous system input. Under the action of the closed-loop control law, the system input in the case of fault mode 2 remains continuous and bounded (see Fig. 10). In Fig. 9(b), the GBNNM model output is equivalent to the

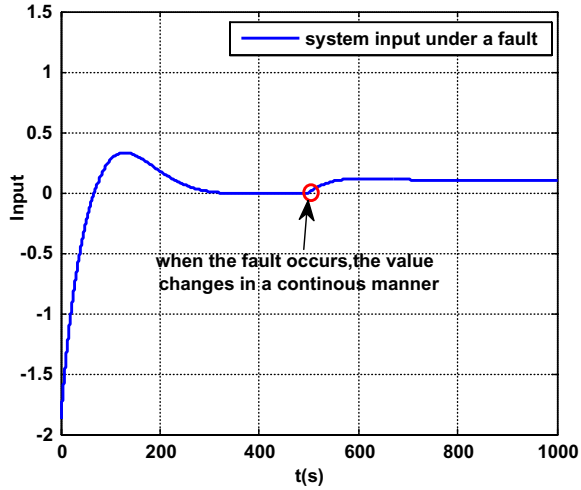

Fig. 10. Input into the RW in the case of fault mode 2.

desired model output, and both outputs are continuous and bounded within the observed time period, $t \in [400, 700]$. Thus, the conditions of Lemma 1 (i.e. continuous and bounded) still hold.

FE for partial LOE and LOE intermittent faults

The sustained faults of different severities are mixed to form intermittent time-varying faults, including partial LOE intermittent faults (fault scenario 1) and LOE intermittent faults (fault scenario 2). In this section, two types of fault scenarios are injected, and simulations based on the FDTCP are used to verify the FE performance subject to intermittent faults of different severities.

Figure 11 illustrates the FE results subjected to fault scenario 1: (a) the response of the system output, (b) the response of the GBNNM model output, and (c) the residual. As shown in Fig. 11(a), the jumps in the system output response at 500, 600, 700 and 800 s demonstrate the effects of fault scenario 1. Under the action of the closed-loop control law, the response curve tends to be steady after these instants. Nevertheless, these data alone cannot determine whether a fault has occurred or the degree of severity of a fault that did occur. In Fig. 11(b), under the same input and fault effect, the response of the GBNNM model output also jumps at a relatively slower speed at 500, 600, 700 and 800 s, and the GBNNM model output is also close to the desired model in normal mode. As shown in Fig. 11(c), the response of the output residual approaches zero in the time interval, $t \in [0 \quad 500]$. When a fault with

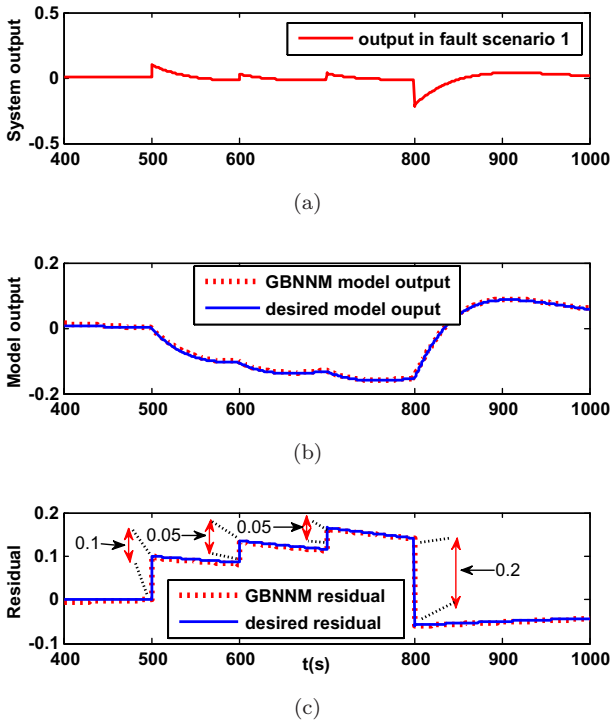

Fig. 11. FE result subjected to fault scenario 1. (a) System output, (b) model output comparison between the desired model and GBNNM, and (c) residual comparison between the desired model and GBNNM.

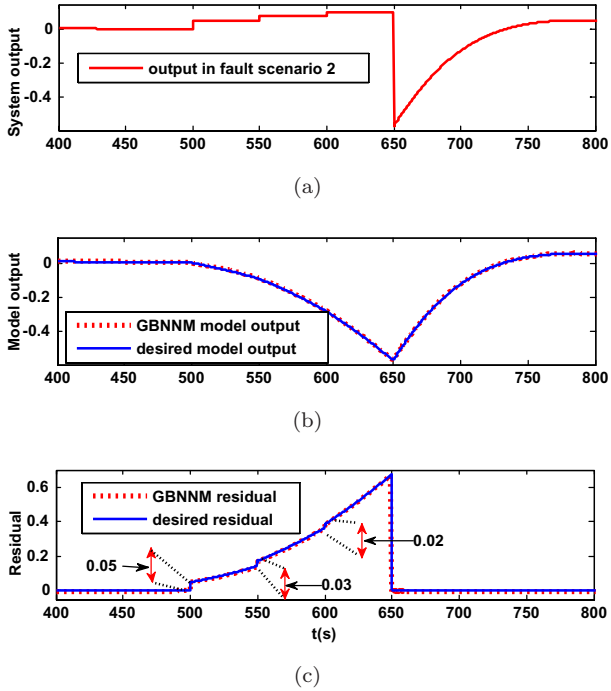

Fig. 12. FE result subject to fault scenario 2. (a) System output, (b) model output comparison between the desired model and GBNNM and (c) residual comparison between the desired model and GBNNM.

value $0.1\,\mathrm{N}\cdot\mathrm{m}$ occurs at 500 s, the value of the residual jumps to a value of $0.1\,\mathrm{N}\cdot\mathrm{m}$, and then tends to be stable under the action of system dynamics. When a fault with a value of $0.15\,\mathrm{N}\cdot\mathrm{m}$ occurs at 600 s, the value of the residual increases $(0.15-0.1=0.05)$ and then tends to be stable. When a fault with a value of $0.2\,\mathrm{N}\cdot\mathrm{m}$ occurs at 700 s, the value of the residual increases $(0.2-0.15=0.05)$ and then tends to be stable. When a fault with a value of $0.2\,\mathrm{N}\cdot\mathrm{m}$ disappears at 800 s, the value of the residual decreases $(0.2-0=0.2)$ and then tends to zero, indicating that the system returns to normal. Based on a theoretical analysis of the nature of a partial LOE fault, the effect of a partial LOE fault tends to decrease under the action of system dynamics. The residual based on the GBNNM reflects not only the severity of the fault at each instance in which a partial LOE fault occurs but also the subsequent potential effects after each fault occurrence for the partial LOE intermittent fault.

The FE result subject to fault scenario 2 is shown in Fig. 12. Based on a theoretical analysis of the nature of an LOE fault, the residual based on the GBNNM reflects not only the severity of the fault in each instance that the LOE fault occurs but also the subsequent potential effects after each fault occurs for the LOE intermittent fault.

(c) Comparisons of GBNNM and other NNs

We now compare our GBNNM with other NNs to demonstrate its superiority for FD. Fault mode 1 with a value of $d^1 = 0.1\,\mathrm{N}\cdot\mathrm{m}$ is injected and simulated to compare several types of major NN-based FD methods, including SNN-, RNN-, PNN- and SPNN-based methods. The best cases of each category are chosen for comparison. The identification effect of these NNs is illustrated in Table 1, and the detailed parameters of these NNs are listed in Table 2. The choice of training data includes two classes: self-defined white noise and normal mode. In the self-defined white noise class, the training data are derived from self-defined white noise exciting input. In the normal mode class, the training data are derived from measurements with a system operating in normal mode.

The FE results based on the SNN, RNN, PNN, SPNN, GBNNM and desired models are shown in

Table 2. Neural network parameters.

Network type		SNN	RNN	PNN	SPNN	GBNNM	
						MLP NN1	MLP NN2
Number of Layers		2	2	2	2	2	2
Properties for Layer 1	Number of neurons	10	10	10	10	10	10
	Transfer function	logsig	tansig	tansig	tansig	tansig	tansig
Properties for Layer 2	Number of neurons	1	1	1	1	1	1
	Transfer function	tansig	tansig	purelin	purelin	purelin	purelin
Dynamic properties	Input delay vector	[a]	[a]	[0 1]	[0 1]	[a]	[a]
	Output delay vector	[a]	[a]	[1 2]	[1 2]	[a]	[a]
Training rules	Training function	TRAINLM	TRAINLM	TRAINLM	TRAINBR	TRAINLM	TRAINLM
	Adaptation learning function	LEARNGDM	LEARNGDM	LEARNGDM	LEARNGDM	LEARNGDM	LEARNGDM
	Performance function	MSE	MSE	MSE	MSE	MSE	MSE
	Choice of training data	Self-defined White-noise	Normal mode	Normal mode	Normal mode	Self-defined White-noise	Self-defined White-noise
Training sample properties	Sample length	1000	1000	1000	1000	1000	1000
	Sampling frequency (Hz/s)	1	1	1	1	1	1

[a]denotes no properties for this option. The expressions of the training function, such as TRAINLM, and the adaptation learning function, such as LEARNGDM, are referred to as the Neural Network Toolbox@matlab.[54] MSE refers to the Mean Square Error.

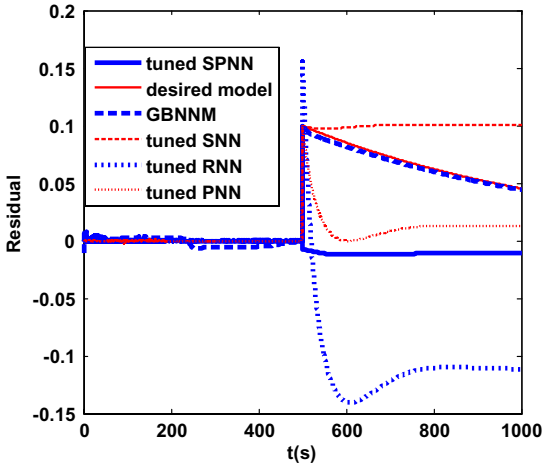

Fig. 13. Residual comparison between the SNN, RNN, PNN, SPNN, desired model and GBNNM.

Fig. 13. To improve the accuracy of the SNN, RNN, PNN and SPNN model residuals, their tuned residuals (i.e. difference of the SNN residuals between the fault mode and fault-free mode) are introduced. As illustrated by the six types of residuals in Fig. 13, the GBNNM residual tracks the desired residual more closely, and does not need to be tuned, which means that the GBNNM has the best accuracy among these models.

***Comment*:** From the FD result and structure of the SNN, we can see that the static NN has no memory, so it can match only static behaviors. From the FD result and the structure of the RNN, PNN and SPNN, we can see that the PNN is the best one among the three dynamic NNs because it has a dynamic structure closest to that of the object system and the effect of unmatched dynamics is the smallest. In contrast, the RNN is the worst choice because its dynamic structure is the most complex and the most different from the object system, and the effect of the unmatched dynamics is strongest. However, none of the choices are sufficiently accurate to fulfill FE as a single NN. Compared with the four NNs, the GBNNM has the ability to conduct FE because it has the best approximation ability and generalization ability, as described in Table 1. The results demonstrate the superiority of the GBNNM in modeling nonlinear dynamic systems.

Compared with several major FD methods based on NN identification, our proposed GBNNM-based MIFE scheme has several advantages. First, system dynamics are considered and matched sufficiently in the GBNNM, and thus, the GBNNM is the closest theoretically to the desired model. Second, the GBNNM can be approximated based on separate parts and is thus easy to implement. Third, the GBNNM residual can be directly used to implement FD, and the residual in fault-free mode is not essential for a better-tuned residual. Finally, the GBNNM residual can quantitatively reflect both the severity of the fault at the occurrence and the subsequent potential effects after its occurrence.

5.4. *LOE FPs estimation result*

To validate the effect of FP estimation using the GBNNM and improved ESO, two partial LOE faults with reference to (16) and (17) are considered in the MIFE scheme. One is the partial LOE sustained fault (fault mode 1) with a value of $d^1 = 0.1\,\mathrm{N\cdot m}$, and the other is the partial LOE intermittent fault (fault mode 1) in the form of (17). Figures 14 and 15 shows the FP estimation results, including estimation of the proposed improved ESO based on NNs (IESONN), estimation of ESO and the real fault value.

As seen from Fig. 14, the curve of the IESONN estimation can accurately indicate the FP value for the partial LOE sustained fault (fault mode 1) with a value of $d^1 = 0.1\,\mathrm{N\cdot m}$. Compared with residual-based diagnosis, the diagnosis effect is more direct and more accurate. Although the IESONN estimation has some error at the fault jumping instant, it

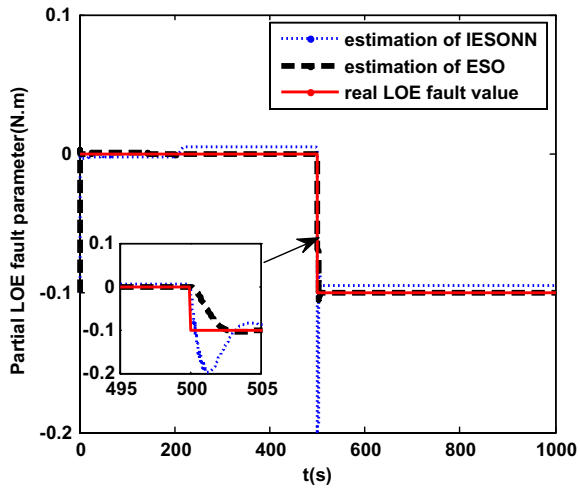

Fig. 14. FP estimation result for a partial LOE sustained fault (fault mode 1) with a value of $d^1 = 0.1\,\mathrm{N\cdot m}$.

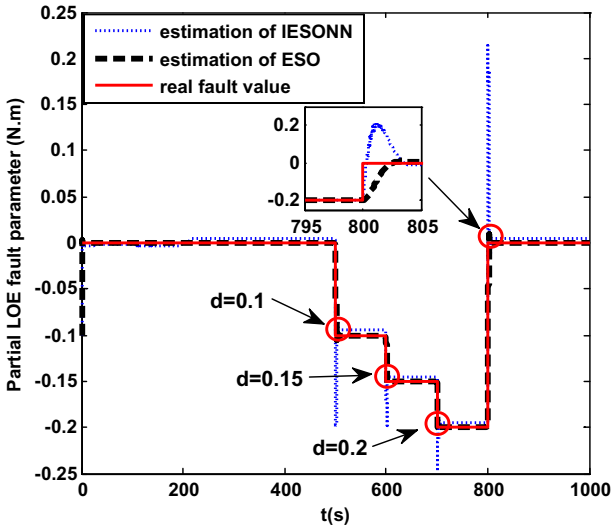

Fig. 15. FP estimation result for a partial LOE sustained fault (fault mode 1) in the form of (17).

will quickly converge to a stable value with the effect of high-gain feedback in the ESO.

As seen from Fig. 15, the IESONN estimation curve can accurately indicate the FP value for the partial LOE intermittent faults (fault mode 1) in the form of (17). A similar conclusion can be drawn: the IESONN estimation can converge to the corresponding stable values at each fault jumping instants.

From the results, we conclude that our IESONN has the same FP estimation ability as the ESO. Because it uses two sub-NNs of the GBNNM to replace the nonlinearity of the object system, it can overcome the limitation of the original ESO when nonlinearity is not available in some practical applications.

6. Conclusions

In this paper, we proposed an MIFE scheme for a general class of nonlinear dynamic systems. In this scheme, a novel GBNNM is constructed from which diagnostic residuals are generated to detect a fault and estimate its severity. Unlike many previously developed NN-based MI methods, our proposed GBNNM is based on system dynamics and is constructed systematically. Thus, it is equivalent to the desired model and suitable for implementation. To estimate the FP for accurate FE, an improved ESO using NNs from the GBNNM is proposed; it has the same estimation ability of the ESO without requiring the knowledge of the nonlinearity of the object system. To illustrate the performance of this MIFE scheme, the model has been applied to the RW of SACS. Test results have demonstrated that this MIFE scheme is effective and optimal for the studied class of nonlinear dynamic systems. Future studies will need to apply the GBNNM to an object system that is more complex and implement fault accommodation based on FE.

Acknowledgments

This work was supported by a grant from the Chinese 863 Program (2007AA04Z438). The authors are grateful to the anonymous reviewers for their helpful comments and suggestions.

References

1. L.-W. Ho and G. G. Yen, Reconfigurable control system design for fault diagnosis and accommodation, *Int. J. Neural Syst.* **12**(6) (2002) 497–520.
2. I. Morgan and H. Liu, Predicting future states with n-dimensional Markov chains for fault diagnosis, *IEEE Trans. Ind. Electron.* **56**(5) (2009) 1774–1781.
3. X. Jiang and H. Adeli, Pseudospectra, MUSIC, and dynamic wavelet neural network for damage detection of highrise buildings, *Int. J. Numer. Methods Eng.* **71**(5) (2007) 606–629.
4. X. Jiang, S. Mahadevan and H. Adeli, Bayesian wavelet packet denoising for structural system identification, *Struct. Control. Health Monit.* **14**(2) (2007) 333–356.
5. B.-H. Cho, J.-S. Jo, S.-J. Joo and H. Kim, Dynamic parameter identification of secondary mass dampers based on full-scale tests, *Comput.-Aided Civ. Infrastruct. Eng.* **27**(3) (2012) 218–230.
6. G. C. Marano, G. Quaranta and G. Monti, Modified genetic algorithm for the dynamic identification of structural systems using incomplete measurements, *Comput.-Aided Civ. Infrastruct. Eng.* **26**(2) (2011) 92–110.
7. U. R. Acharya, R. Yanti, J. W. Zheng, M. M. R. Krishnan, J. H. Tan, R. J. Martis and C. M. Lim, Automated diagnosis of epilepsy using cwt, hos and texture parameters, *Int. J. Neural Syst.* **23**(3) (2013) 1350009.
8. R. J. Martis, U. R. Acharya, L. C. Min, K. M. Mandana, A. K. Ray and C. Chakraborty, Application of higher order cumulant features for cardiac health diagnosis using ECG signals, *Int. J. Neural Syst.* **23**(4) (2013) 1350014.
9. Y. Yi, L. Guo and H. Wang, Adaptive statistic tracking control based on two-step neural networks with time delays, *IEEE Trans. Neural Netw.* **20**(3) (2009) 420–429.

10. M. Chow, G. Bilbro and S. O. Yee, Application of learning theory to an artificial neural network that detects incipient faults in single-phase induction motors, *Int. J. Neural Syst.* **91**(2) (1991) 91–100.
11. E. D. Wandekokem, E. Mendel, F. Fabris, M. Valentim, R. J. Batista, F. M. Varejão and T. W. Rauber, Diagnosing multiple faults in oil rig motor pumps using support vector machine classifier ensembles, *Integr. Comput. Aided Eng.* **18**(1) (2011) 61–74.
12. A. Alvanchi, S. Lee and S. AbouRizk, Modeling framework and architecture of hybrid system dynamics and discrete event simulation for construction, *Comput.-Aided Civ. Infrastruct. Eng.* **26**(2) (2011) 77–91.
13. F. Ahmadkhanlou and H. Adeli, Optimum cost design of reinforced concrete slabs using neural dynamics model, *Eng. Appl. Artif. Intell.* **18**(1) (2005) 65–72.
14. H. Adeli and H. S. Park, A neural dynamics model for structural optimization — Theory, *Comput. Struct.* **57**(3) (1995) 383–390.
15. H. Adeli and H. S. Park, Optimization of space structures by neural dynamics, *Neural Netw.* **8**(5) (1995) 769–781.
16. H. S. Park and H. Adeli, A neural dynamics model for structural optimization application to plastic design of structures, *Comput. Struct.* **57**(3) (1995) 391–399.
17. H. S. Park and H. Adeli, Distributed neural dynamics algorithms for optimization of large steel structures, *J. Struct. Eng.* **123**(7) (1997) 880–888.
18. H. Adeli and A. Karim, Scheduling/cost optimization and neural dynamics model for construction, *J. Constr. Eng. Manage.* **123**(4) (1997) 450–458.
19. A. B. Senouci and H. Adeli, Resource scheduling using neural dynamics model of Adeli and Park, *J. Constr. Eng. Manage.* **127**(1) (2001) 28–34.
20. H. Adeli and H. Kim, Cost optimization of composite floors using neural dynamics model, *Commun. Numer. Methods Eng.* **17**(11) (2001) 771–787.
21. A. Tashakori and H. Adeli, Optimum design of cold-formed steel space structures using neural dynamics model, *J. Constr. Steel Res.* **58**(12) (2002) 1545–1566.
22. D.-Y. Lin, A Dual Variable approximation-based descent method for a bi-level continuous dynamic network design problem, *Comput.-Aided Civ. Infrastruct. Eng.* **26**(8) (2011) 581–594.
23. A. Khashman, Blood cell identification using a simple neural network, *Int. J. Neural Syst.* **18**(5) (2008) 453–458.
24. N. Wang, M. J. Er, X. Y. Meng and X. Li, An online self-organizing scheme for parsimonious and accurate fuzzy neural networks, *Int. J. Neural Syst.* **20**(5) (2010) 389–403.
25. S. Wu and T. W. S. Chow, Induction machine fault detection using SOM-based RBF neural networks, *IEEE Trans. Ind. Electron.* **51**(1) (2004) 183–194.
26. H. Su and K. T. Chong, Induction machine condition monitoring using neural network modeling, *IEEE Trans. Ind. Electron.* **54**(1) (2007) 241–249.
27. R. J. Patton, C. J. Lopez-Toribio and F. J. Uppal, Artificial intelligence approaches to fault diagnosis for dynamic systems, *Appl. Math. Comput.* **9** (1999) 471–518.
28. G. Puscasu and B. Codres, Nonlinear system identification and control based on modular neural networks, *Int. J. Neural Syst.* **21**(4) (2011) 319–334.
29. K. S. Narendra and K. Parthasarathy, Identification and control of dynamical systems using neural networks, *IEEE Trans. Neural Netw.* **1**(1) (1990) 4–27.
30. G. Puscasu, B. Codres, A. Stancu and G. Murariu, Nonlinear system identification based on internal recurrent neural networks, *Int. J. Neural Syst.* **19**(2) (2009) 115–125.
31. X.-D. Li, J. K. L. Ho and T. W. S. Chow, Approximation of dynamical time-variant systems by continuous-time recurrent neural networks, *IEEE Trans. Circuits Syst. II* **52**(10) (2005) 656–660.
32. S. Freitag, W. Graf and M. Kaliske, Recurrent neural networks for fuzzy data, *Integr. Comput. Aided Eng.* **18**(3) (2011) 265–280.
33. A. Yazdizadeh and K. Khorasani, Nonlinear system identification using embedded dynamic neural networks, in *Proc. Int. Joint Conf. Neural Networks* (*IJCNN*) (1998), pp. 378–383.
34. F. Abdollahi, H. A. Talebi and R. V. Patel, Stable identification of nonlinear systems using neural networks: Theory and experiments, *IEEE/ASME Trans. Mechatron.* **11**(4) (2006) 488–495.
35. X. Jiang and H. Adeli, Dynamic wavelet neural network for nonlinear identification of highrise buildings, *Comput.-Aided Civ. Infrastruct. Eng.* **20**(5) (2005) 316–330.
36. H. Adeli and X. Jiang, Dynamic fuzzy wavelet neural network model for structural system identification, *J. Struct. Eng.* **132**(1) (2006) 102–111.
37. D. Theodoridis, Y. Boutalis and M. Christodoulou, Dynamical recurrent neuro-fuzzy identification schemes employing switching parameter hopping, *Int. J. Neural Syst.* **22**(2) (2012).
38. E. B. Kosmatopoulos, M. M. Polycarpou, M. A. Christodoulou and P. A. Ioannou, High-order neural network structures for identification of dynamical systems, *IEEE Trans. Neural Netw.* **6**(2) (1995) 422–431.
39. J. A. Ruz-Hernandez, E. N. Sanchez and D. A. Suarez, Optimal training for associative memories: Application to fault diagnosis in fossil electric power plants, in *Hybrid Intelligent Systems* (Springer, 2007), pp. 329–356.

40. X. Jiang and H. Adeli, Dynamic wavelet neural network model for traffic flow forecasting, *J. Transp. Eng.* **131**(10) (2005) 771–779.
41. Y. H. Kim, F. L. Lewis and C. T. Abdallah, Nonlinear observer design using dynamic recurrent neural networks, in *35th IEEE Conf. Decision and Control*, *CDC* (1996), pp. 949–954.
42. H. A. Talebi, K. Khorasani and S. Tafazoli, A recurrent neural-network-based sensor and actuator fault detection and isolation for nonlinear systems with application to the satellite's attitude control subsystem, *IEEE Trans. Neural Netw.* **20**(1) (2009) 45–60.
43. E. Sobhani-Tehrani and K. Khorasani, *Fault Diagnosis of Nonlinear Systems Using a Hybrid Approach* (Springer Verlag, 2009).
44. E. Sobhani-Tehrani, H. A. Talebi and K. Khorasani, A nonlinear hybrid fault detection, isolation and estimation using bank of neural parameter estimators, in *Proc. of the 17th IFAC World Congress* (2008), pp. 7251–7258.
45. X. Hong and S. Chen, Modeling of complex-valued Wiener systems using B-spline neural network, *IEEE Trans. Neural Netw.* **22**(5) (2011) 818–825.
46. X. Hong and S. Chen, The system identification and control of Hammerstein system using non-uniform rational B-spline neural network and particle swarm optimization, *Neurocomputing* **82** (2012) 216–223.
47. Z. Q. Li, L. Ma and K. Khorasani, Fault diagnosis of an actuator in the attitude control subsystem of a satellite using neural networks, in *Proc. Int. Joint Conf. Neural Networks* (*IJCNN*) (2007), pp. 2658–2663.
48. N. Tudoroiu and K. Khorasani, Satellite fault diagnosis using a bank of interacting Kalman filters, *IEEE Trans. Aerosp. Electron. Syst.* **43**(4) (2007) 1334–1350.
49. Z. Cen, J. Wei and R. Jiang, Fault diagnosis based on grey-box neural network identification model, in *Proc. Int. Conf. Control Automation and Systems* (*ICCAS*) (2010), pp. 249–254.
50. Z. Cen, J. Wei and R. Jiang, A Grey-Box Neural Network based identification model for nonlinear dynamic systems, in *Proc. of the Fourth Int. Workshop on Advanced Computational Intelligence* (*IWACI*) (2011), pp. 300–307.
51. Z. Cen, J. Wei, R. Jiang and X. Liu, Diagnosis for actuator partial LOE Fault in Dynamic System with nonlinear actuator, in *Proc. of The 29th Chinese Control Conference* (*CCC*) (2010), pp. 3993–3999.
52. D. P. Mandic and J. Chambers, *Recurrent Neural Networks for Prediction*: *Learning Algorithms*, *Architectures and Stability* (John Wiley & Sons, Inc., 2001).
53. J. Sjöberg, Q. Zhang, L. Ljung, A. Benveniste, B. Delyon, P.-Y. Glorennec, H. Hjalmarsson and A. Juditsky, Nonlinear black-box modeling in system identification: A unified overview, *Automatica* **31**(12) (1995) 1691–1724.
54. H. Demuth and M. Beale, *Neural network toolbox for use with MATLAB* (The Math Works, 1993).
55. Z. Cen, J. Wei, R. Jiang and T. Yan, Accurate diagnosis on process fault parameters of nonlinear actuator based on adaptive observer and extended state observer, *J. Astronaut.* **32**(6) (2011) 1318–1326.
56. H. Liao, Studies on the attitude determination and control system of an earth-oriented three-axis stabilized satellite, Ph. D. monogram dissertation, Department of Aerospace Engineering, Northwestern Polytechnical University, Xian, China (2000).
57. X. Wang and M. Ni, An adaptive observer based fault diagnosis for nonlinear systems, *Aerospace Contr. Appl.* **34**(4) (2008) 33–37.
58. Z. Li, Y. Hao, J. Tu and X. Wang, Fault simulation platform of satellite attitude control system based on embedded simulation, *J. Shandong University* (*Eng. Sci.*) **35**(3) (2005) 88–92.